

# Robust Detection of Premature Ventricular Contractions Using a Wave-Based Bayesian Framework

Omid Sayadi\*, *Student Member, IEEE*, Mohammad B. Shamsollahi, *Member, IEEE*, and Gari D. Clifford, *Senior Member, IEEE*

**Abstract**—Detection and classification of ventricular complexes from the ECG is of considerable importance in Holter and critical care patient monitoring, being essential for the timely diagnosis of dangerous heart conditions. Accurate detection of premature ventricular contractions (PVCs) is particularly important in relation to life-threatening arrhythmias. In this paper, we introduce a model-based dynamic algorithm for tracking the ECG characteristic waveforms using an extended Kalman filter. The algorithm can work on single or multiple leads. A “polargram”—a polar representation of the signal—is introduced, which is constructed using the Bayesian estimations of the state variables. The polargram allows the specification of a polar envelope for normal rhythms. Moreover, we propose a novel measure of signal fidelity by monitoring the covariance matrix of the innovation signals throughout the filtering procedure. PVCs are detected by simultaneous tracking the signal fidelity and the polar envelope. Five databases, including 40 records from MIT-BIH arrhythmia database, are used for differentiating normal, PVC, and other beats. Performance evaluation results show that the proposed method has an average detection accuracy of 99.10%, aggregate sensitivity of 98.77%, and aggregate positive predictivity of 97.47%. Furthermore, the method is capable of 100% accuracy for records that contain only PVCs and normal sinus beats. The results illustrate that the method can contribute to, and enhance the performance of clinical PVC detection.

**Index Terms**—Characteristic waves, ECG, extended Kalman filter (EKF), premature ventricular contraction (PVC), signal fidelity, signal quality, wave-based dynamical model.

## I. INTRODUCTION

CARDIOVASCULAR diseases (CVDs) are the leading single cause of death in the developed world and are responsible for more than 30% of all deaths in most countries. For instance, the American Heart Association (AHA) recently reported that nearly 80 million people in the U.S. were burdened by some form of CVD, of which eight million experienced myocardial infarction, or a “heart attack.” Additionally, CVDs were the underlying cause of 1 in every 2.8 deaths in 2008 [1]. The

detection of CVD and the determination of the underlying etiology of the disease for prevention and treatment is therefore a crucial task. Identifying premature ventricular contractions (PVCs) in Holter recordings or during monitoring is of particular interest. PVCs result from irritated ectopic foci in the heart’s ventricles, and are independent of the pace set by the sinoatrial node. Recent studies have shown that the occurrence of PVCs is indicative of increased risk of sudden cardiac death, and is linked to mortality when associated with myocardial infarction [2]. The presence of PVCs has also been shown to be associated with an increased total mortality in some patient subgroups, suggesting that a high frequency of PVCs is a marker of a more severe disease process, rather than the provocateur of a terminal electrical event. Events that occur after a PVC are also of interest, and in particular, the rate of acceleration and deceleration of the heart rate immediately after a PVC has shown to be more effective than ejection fraction in stratifying patients postmyocardial infarction [3]. Therefore, accurate detection of PVCs is of great significance for stratifying patients at high risk and predicting life-threatening ventricular arrhythmias.

Accurate, noninvasive diagnosis of and screening for CVD has been a challenge. ECG analysis is routinely used as the first tool for initial screening and diagnosis in clinical practice. The ECG as a noninvasive and low-cost method provides valuable clinical information regarding the rate, timing and regularity of the heart [4]. Analysis of the ECG remains the benchmark method for cardiac arrhythmia detection. Several methods have been proposed in the literature for automatic detection and classification of various arrhythmias. The vast majority of the developed techniques includes algorithms based on time-domain features [5], ECG morphology and heartbeat interval features [6], principal component analysis (PCA) [7], hidden Markov models [8]–[10], self-organizing maps [11], wavelets and filter banks [12], [13], statistical classifiers [14], and neural networks (NNs) [15], [16]. On the other hand, efforts have been aimed at coping with the specific problem of PVC detection. Most works in this field employ NNs to classify the PVCs after performing a suitable processing for the extraction of discriminant features [17]–[22], and some authors underline the advantages of the competitive classifiers [18], [23]. Although these methods have shown promising results, they have several disadvantages. First, the methods suffer from the problem of finding efficient feature sets [19]–[22]. Second, since there are various choices for selecting the network structure to achieve an acceptable performance, finding the optimum architecture has

Manuscript received May 27, 2009; revised July 25, 2009. First published September 15, 2009; current version published January 20, 2010. *Asterisk indicates corresponding author.*

\*O. Sayadi is with the Biomedical Signal and Image Processing Laboratory, School of Electrical Engineering, Sharif University of Technology, Tehran 11365-9363, Iran (e-mail: osayadi@ee.sharif.edu).

M. B. Shamsollahi is with the Biomedical Signal and Image Processing Laboratory, School of Electrical Engineering, Sharif University of Technology, Tehran 11365-9363, Iran (e-mail: mbshams@sharif.edu).

G. D. Clifford is with the Institute of Biomedical Engineering, Department of Engineering Science, University of Oxford, OX3 7DQ, U.K. (e-mail: gari@robots.ox.ac.uk).

Digital Object Identifier 10.1109/TBME.2009.2031243

not a unique solution [20]–[22]. The use of symbolic dynamics analysis [24] and Gaussian processes [25] for PVC detection has also been reported.

Recently, Bayesian filters were proposed for ECG denoising [26] and filtering cardiac contaminants [27]. The state-space model used in this approach was inspired from the model proposed by McSharry *et al.* [28], who suggested the use of Gaussian mixture models to generate synthetic ECGs. It was later found that by some modifications, the filtering framework developed by Clifford *et al.* [29] and Sameni *et al.* [26] could be used as a parameter-based framework for model-based ECG filtering [29], [30], simultaneous denoising and compression [29], [31], and beat segmentation [29], [32].

In this paper, we propose the tracking of the parameters of an updated Gaussian wave-based representation of the ECG by employing a Bayesian estimation procedure through an extended Kalman filter (EKF). A new polar representation is then introduced together with a procedure to track rhythm changes using the innovation sequence provided by the EKF. The paper is organized as follows. In Section II, the wave-based dynamical model is presented. Section III provides relevant background on the theory of the EKF. In Section IV, our proposed algorithm for PVC detection is explained in detail. Section V is devoted to simulation results. Finally, discussion and conclusions are provided in Section VI.

## II. WAVE-BASED ECG DYNAMICAL MODEL

A simple interpretation for modeling an ECG record is to model every heart beat as a combination of finite characteristic waveforms (CWs), each of which represented by the sum of Gaussian kernels. In other words, we assume that every cycle of a heartbeat recorded on an ECG can comprise a finite number of CWs (typically the P wave, QRS complex, and T wave). However, every CW reflects the electrophysiologic functioning of a specific part of the heart, which, in turn, facilitates the analysis of the ECG events. This idea originates from the synthetic nonlinear dynamic model that was proposed for generating artificial ECGs by McSharry *et al.* [28]. The model generates a 3-D trajectory that consists of a circular limit cycle that is pushed up and down as it approaches each of the turning points in the ECG ( $P$ ,  $Q$ ,  $R$ ,  $S$ , and  $T$ ) whose centers are the center of each Gaussian. The simplified discrete version of the model in the polar plane is given by [26]

$$\begin{cases} \varphi_{k+1} = (\varphi_k + \omega\delta) \bmod (2\pi) \\ s_{k+1} = s_k - \sum_{i \in \{P, Q, R, S, T\}} \delta \frac{\alpha_{i_k} \omega}{b_{i_k}^2} \Delta\theta_{i_k} \exp\left(-\frac{\Delta\theta_{i_k}^2}{2b_{i_k}^2}\right) + \eta_k \end{cases} \quad (1)$$

where  $\delta$  is the sampling period,  $\omega = 2\pi f$ ,  $f$  is the beat-to-beat heart rate and  $\Delta\theta_{i_k} = (\varphi_k - \theta_{i_k}) \bmod (2\pi)$ . The phase  $\varphi$  is a saw-tooth shape signal that is expected to be zero at R-peaks, and is linearly assigned a value between  $-\pi$  and  $\pi$  for each sample between two successive R-peaks.  $\alpha_i$ ,  $b_i$ , and  $\theta_i$  are the amplitude, angular spread, and location of the Gaussian functions, respectively, and  $\eta$  represents random additive white noise that accounts for baseline wander effects and other additive sources

of process noise. It can be seen that the ECG signal  $s$  is represented by a sum of Gaussian functions, whose locations are controlled by the phase signal  $\varphi$ . In order to model the separate events of an ECG signal, the second dynamical equation in (1) can be divided into separate state variables, each of which has a similar behavior to the original equation. However, the separation and the corresponding increase in the dimensionality facilitate the analysis of different events in the ECG signal.

Assuming the presence of three distinct CWs, corresponding to the P wave, QRS complex, and T wave, the ECG signal is divided into three components. In addition, to have a more accurate representation of the CWs, the number of Gaussian functions can be varied. Clifford *et al.* proposed an extension of the model that used an arbitrary number of Gaussians, with 2 Gaussians for each asymmetric turning point ( $P$  and  $T$ ) [29]. Since Gaussians are symmetric, asymmetric turning points require more than one Gaussian and that two is the minimum number in this case, and therefore, the best choice, as we want to minimize the number of parameters for computational simplicity. Accordingly, P wave and T wave are characterized by two Gaussian kernels to account for biphasic P waves and the asymmetric nature of the T wave at low-to-medium heart rates. In contrast, the inclusion of more than one kernel for Q, R, and S is of negligible importance. Specifically, Sayadi and Shamsollahi showed that minimum five kernels are essential for preserving the morphological features in the EKF-filtered signal [31]. However, increasing the number of Gaussians has a negligible effect on the filtering performance, yet provides a slightly improved compression ratio [30], [31]. Consequently, we adopted seven Gaussian kernels to model an ECG beat. The modified model is given by

$$\begin{cases} \varphi_{k+1} = (\varphi_k + \omega\delta) \bmod (2\pi) \\ P_{k+1} = P_k - \sum_{i \in \{P^-, P^+\}} \delta \frac{\alpha_{i_k} \omega}{b_{i_k}^2} \Delta\theta_{i_k} \exp\left(-\frac{\Delta\theta_{i_k}^2}{2b_{i_k}^2}\right) + \eta_{P_k} \\ C_{k+1} = C_k - \sum_{i \in \{Q, R, S\}} \delta \frac{\alpha_{i_k} \omega}{b_{i_k}^2} \Delta\theta_{i_k} \exp\left(-\frac{\Delta\theta_{i_k}^2}{2b_{i_k}^2}\right) + \eta_{C_k} \\ T_{k+1} = T_k - \sum_{i \in \{T^-, T^+\}} \delta \frac{\alpha_{i_k} \omega}{b_{i_k}^2} \Delta\theta_{i_k} \exp\left(-\frac{\Delta\theta_{i_k}^2}{2b_{i_k}^2}\right) + \eta_{T_k} \end{cases} \quad (2)$$

where  $\eta_P$ ,  $\eta_C$ , and  $\eta_T$  represent the baseline perturbations of the P wave, QRS complex, and T wave, respectively.

## III. BAYESIAN STATE ESTIMATION THROUGH EKF

Having derived the state-space representation for the ECG signal, the process equations of a Bayesian framework are formed. Relating the ECG signal as an observation to the state variables in the left side of model (2) is now straightforward, since the CWs are summed up to form the ECG. The observed noisy phase  $\phi_k$  and noisy amplitude  $z_k$  of the ECG are given by:

$$\begin{cases} \phi_k = \varphi_k + u_{1_k} \\ z_k = P_k + C_k + T_k + u_{2_k} \end{cases} \quad (3)$$

where  $u_{1k}$  and  $u_{2k}$  are the observation noises of the ECG in the phase and spatial domains, respectively. Using the wave-based dynamical model (2) as the process equations and the observation relations (3), the state variables vector  $\underline{x}_k$  and the observation vector  $y_k$ , and the process noise vector  $\underline{w}_k$  and the observation noise vector  $\underline{v}_k$ , are defined, respectively, as

$$\begin{aligned}\underline{x}_k &= [\varphi_k \quad P_k \quad C_k \quad T_k]' \\ \underline{y}_k &= [\phi_k \quad z_k]' \\ \underline{w}_k &= [\alpha_{i_k}, b_{i_k}, \theta_{i_k}, \omega, \eta_{P_k}, \eta_{C_k}, \eta_{T_k}]', \\ &\quad i \in \{P^-, P^+, Q, R, S, T^-, T^+\} \\ \underline{v}_k &= [u_{1k} \quad u_{2k}]'. \end{aligned} \quad (4)$$

The wave-based dynamic model [see (2)] is a nonlinear function of the state and process noise vectors. Therefore, nonlinear extensions of the Kalman filter (KF) are required for estimating the state vector. Our proposed framework is built upon an EKF structure for its simplicity and improved numerical stability over other Bayesian filters [33]. In order to use the KF formalism for this system, it is necessary to derive a linear approximation of (2) near a desired reference point  $(\hat{x}_k, \hat{w}_k, \hat{v}_k)$ , to obtain the following linear approximate model:

$$\begin{cases} \underline{x}_{k+1} = f(\underline{x}_k, \underline{w}_k, k) \\ \quad \approx f(\hat{x}_k, \hat{w}_k, k) + A_k(\underline{x}_k - \hat{x}_k) + B_k(\underline{w}_k - \hat{w}_k) \\ \underline{y}_k = g(\underline{x}_k, \underline{v}_k, k) \\ \quad \approx g(\hat{x}_k, \hat{v}_k, k) + M_k(\underline{x}_k - \hat{x}_k) + N_k(\underline{v}_k - \hat{v}_k) \end{cases} \quad (5)$$

where  $f$  is the state evolution function and  $g$  represents the relationship between the states and the observations [see (2), (3)]. The linear approximate coefficients in (5) are given by [34]

$$\begin{aligned} A_k &= \left. \frac{\partial f(\underline{x}, \underline{w}, k)}{\partial \underline{x}} \right|_{\underline{x}=\hat{x}_k} & B_k &= \left. \frac{\partial f(\hat{x}_k, \underline{w}, k)}{\partial \underline{w}} \right|_{\underline{w}=\hat{w}_k} \\ M_k &= \left. \frac{\partial g(\underline{x}, \underline{v}, k)}{\partial \underline{x}} \right|_{\underline{x}=\hat{x}_k} & N_k &= \left. \frac{\partial g(\hat{x}_k, \underline{v}, k)}{\partial \underline{v}} \right|_{\underline{v}=\hat{v}_k} \end{aligned} \quad (6)$$

In order to implement the EKF, the time propagation and the measurement propagation equations are summarized as [34]:

$$\begin{cases} \hat{x}_k^- = f(\hat{x}_{k-1}^+, \underline{w}, k) \Big|_{\underline{w}=0} \\ H_k^- = A_{k-1} H_{k-1}^+ A_{k-1}' + B_{k-1} Q_{k-1} B_{k-1}', \\ \hat{x}_k^+ = \hat{x}_k^- + K_k r_k \\ K_k = H_k^- M_k' [M_k H_k^- M_k' + N_k R_k N_k']^{-1} \\ \underline{r}_k = y_k - g(\hat{x}_k^-, \underline{v}, k) \Big|_{\underline{v}=0} \\ H_k^+ = H_k^- - K_k M_k H_k^- \end{cases} \quad (7)$$

where  $\hat{x}_k^- = \hat{E}\{x_k | y_{k-1}, \dots, y_1\}$  is its *a priori* estimate  $x_k$ , at the  $k$ th stage using the observations  $y_1$  to  $y_{k-1}$ , and  $\hat{x}_k^+ = \hat{E}\{x_k | y_k, \dots, y_1\}$  is its *a posteriori* estimate after using the  $k$ th observation  $y_k$ .  $H_k^-$  and  $H_k^+$  are defined in the same manner to be the estimations of the covariance matrices, in the  $k$ th stage, before and after using the  $k$ th observation, respectively. In addition,  $Q_k = E\{w_k w_k^T\}$  and  $R_k = E\{v_k v_k^T\}$  are the covariance matrices of the process noises and measurement noises,

respectively, and  $\bar{w}_k = E\{w_k\}$ ,  $\bar{v}_k = E\{v_k\}$  [35]. As it can be seen in (7), the key idea of the EKF is to linearize the nonlinear system model in the vicinity of the previous estimated point, and to recursively calculate the filter gain  $K_k$ , the innovation signal  $\underline{r}_k$  and the state covariance matrices  $H_k^-$  and  $H_k^+$  from the linearized equations, while the KF time propagation is performed via the original nonlinear equations [36].

#### IV. BAYESIAN DETECTION OF PVC

A PVC is a morphological abnormality that generally only appears in a small number of the ECG cycles and imposes a rhythm change in the normal ECG pattern, so that the P wave vanishes by the occurrence of a dominant wide QRS followed by a dominant T wave. This morphological change can lead to large errors in the Gaussians functions' locations. In this case, the EKF estimations are not expected to be satisfactory. However, the benefit of the Gaussian mixture representation is that the effect of each Gaussian term vanishes very quickly (in less than the ECG period), meaning that the errors are not propagated to the following ECG beats [26]. Moreover, by monitoring the state estimates' covariance matrices and the variations of the innovation signals, it is possible to detect such unexpected abnormalities. Therefore, in this section, we define some signal fidelities by tracking the covariance matrix  $r_k$  throughout the filtering procedure to detect unexpected morphological changes, such as a PVC. We also introduce a new polar representation to distinguish PVCs from other rhythm changes.

##### A. Monitoring Signal Fidelity

In practice, due to the Gaussian assumption on the noise sources and the initial state vector values, the state estimate entries of  $\hat{x}_k^+$  should lie within the envelope of the square roots of their corresponding diagonal entries in  $H_k^+$  for the majority of the time. Hence, by monitoring the variance of the state estimates, it is possible to detect these morphological changes [33].

Another approach to provide a means of monitoring the fidelity of the filter is to update the values of  $Q_k$  and  $R_k$ , which is practically convenient to monitor the covariance matrix of the innovation signal throughout the filtering and to compare it to the innovation covariance matrices estimated by the KF [37]. Specifically, with a diagonal (or diagonalized) noise covariance matrix of  $R_k$ , the following term can be formed for the  $i$ th ECG measurement, which we call the signal fidelity

$$\gamma_i^{\text{CW}} = \frac{1}{N} \sum_{k=i-N+1}^i \frac{(r_k^s)^2}{E\{(r_k^{\text{CW}})^2\}}, \quad \text{CW} \in \{P, C, T\} \quad (8)$$

where  $r_k^s$  is the second entry of the zero-mean innovation vector of  $\underline{r}_k$  defined in (6), corresponding to the  $k$ th ECG measurement,  $N$  is the length of the averaging window, and  $E\{(r_k^{\text{CW}})^2\}$  is the KF estimated variance of  $r_k^s$  for CWs, given by

$$E\{(r_k^{\text{CW}})^2\} = (\underline{M}_k^s (H_k^-)^{\text{CW}}) m_k^{\text{CW}} + \sigma_{u_{2k}}^2 \quad (9)$$

where  $\underline{M}_k^s$  is the second row of the  $M_k$  matrix defined in (7),  $m_k^P$ ,  $m_k^C$ , and  $m_k^T$  are the second, third, and fourth entry of  $\underline{M}_k^s$ , respectively. Similarly,  $(H_k^-)^P$ ,  $(H_k^-)^C$ , and  $(H_k^-)^T$  are the second, third and fourth column of the  $H_k^-$  matrix, respectively, and  $\sigma_{u_{2k}}^2 = E\{u_{2k}^2\}$  is the second diagonal entry of  $R_k$ .

In fact,  $\gamma^{CW}$  is an average of the variances of the  $N$  recent ECG innovations, normalized by their KF estimated variances of the corresponding CWs. This formulation originates from the proposal of Sameni *et al.* [26] to use the KF estimated variance for improving the filtering performance. However, since we are intended to investigate the fidelity for every characteristic component, in the current approach, the original formulation is modified to provide three signal fidelities corresponding to three CWs. It is worth noting that as long as the ECG morphology remains normal,  $\gamma_i \approx 1$ . Values much greater than unity indicate that the innovation signal variance is being underestimated by the KF, while values close to zero indicate that the innovation signal variance is being overestimated. Sameni *et al.* benefited from this property of  $\gamma_i$  to adaptively modify the KF noise parameters to ensure the filter stability and to achieve better filtering performances in low SNR scenarios [26]. However, in the current approach, we monitor the  $\gamma^{CW}$ 's to detect any significant rhythm change in the ECG signal, which will affect the P-QRS-T morphology. In addition, unlike the original model (1), the wave-based model (2) enables us to define three  $\gamma^{CW}$  corresponding to each CW. Hence, the morphological changes may be simply identified and localized by monitoring the  $\gamma^{CW}$  signals. Three adaptive thresholds,  $\text{thr}^{CW}$ , corresponding to three  $\gamma^{CW}$  signals are used to detect the fidelity peaks. The value of  $\text{thr}^{CW}$  is defined to preserve 95% of the  $\gamma^{CW}$  energy, and is at least three times the mean value of  $\gamma^{CW}$ . In other words, with  $L$  be the length of the signal fidelity, the thresholds should satisfy the following conditions:

$$\begin{cases} \text{thr}^{CW} \geq 3\bar{\gamma}^{CW} \\ \forall j \ni \gamma_j^{CW} \leq \text{thr}^{CW} : \sum_j |\gamma_j^{CW}|^2 = 0.95 \sum_{i=1}^L |\gamma_i^{CW}|^2. \end{cases} \quad (10)$$

The best values of the energy and multiplier of the mean value of  $\gamma^{CW}$  were found by changing all possible values over the used database.

As a disadvantage, the innovation sequences are affected not only by morphological changes of the observation signals, but also by local noise artifacts and filter divergences [37]. Hence, in order to identify the PVCs using  $\gamma^{CW}$ , we need a symptom of rhythm change for discrimination between artifacts and real rhythm changes. In the next section, we introduce a polar representation using the estimations provided by the EKF and address how to use this representation for PVC rhythm identification.

### B. Polargram Formation and Envelope Extraction

The wave-based ECG dynamical model (2) suggests that the ECG signal is considered as a combination of three characteristic waveforms. Using a Bayesian filter structure, each of these CWs, as well as the phase signal, can be tracked in time. A polar representation for the ECG signal, which we call *polargram*,

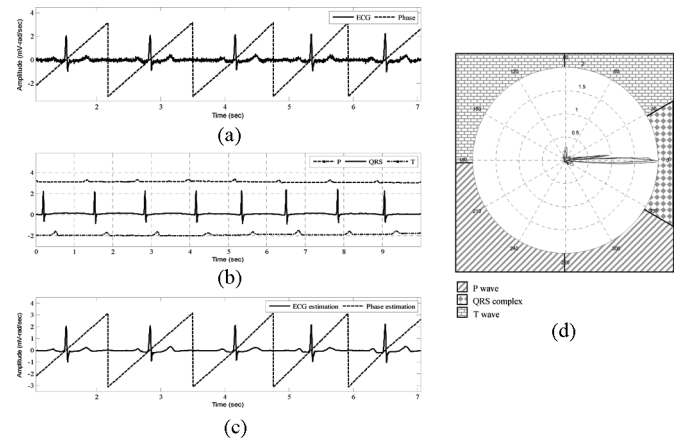


Fig. 1. EKF estimations and polargram formation for a typical normal ECG signal. (a) ECG noisy record and the corresponding phase signal. (b) CW estimation provided by EKF4. (c) Estimated phase and filtered ECG signals using EKF4. (d) Polargram with the CW partitioning included.

can be obtained using the 2-D vector  $[\varphi_k (P + C + T)_k]'$  at each time instance,  $k$ . By simply plotting the samples of the summed CWs, as the amplitude, and their corresponding phase values, a polargram for the whole ECG signal is obtained. The polargram clearly shows the beat-to-beat variations during different ECG cycles. In addition, by analyzing a specific portion of the polar plane, it is possible to investigate the interbeat variations for every CW. This is because in the phase signal construction, the R-peak is always assumed to be located at  $\theta_R = 0$  and the ECG contents lying between two consecutive R-peaks are assumed to have a phase between  $-\pi$  and  $\pi$  [26]. Visual inspection of various ECG signals shows that the QRS complex lies in the range of  $[-\pi/6, \pi/6]$ . Hence, the preceding P wave and the proceeding T wave will occur in the range of  $[-\pi, -\pi/6]$  and  $[\pi/6, \pi]$ , respectively. Fig. 1 shows a typical normal ECG signal and the corresponding phase signal, the estimations provided by the EKF and the polargram with the corresponding partitioning. In fact, the polargram is simply the polar plot of  $(P + C + T)_k$  versus  $\varphi_k$ , and the idea of partitioning the polargram is the key to identifying PVCs from normal sinus beats.

As stated before, the morphological changes imposed by PVC leads to large errors in the Gaussian kernels' locations, which result in unsatisfactory filtering performance. In other words, the PVC morphology has minimum amount of phase overlap with the underlying morphology of the normal ECG signal. Hence, if we specify a specific span in the polargram, any undesired change in the morphology of the signal would lie out of this span. Using the mean  $[\overline{ECG}(\theta)]$  and the standard deviation  $[\sigma_{ECG}(\theta)]$  of this new representation, we define a polar envelope that spans between the upper and lower ranges of  $\overline{ECG}(\theta) \pm 3\sigma_{ECG}(\theta)$  in the polar plane. Hence, any morphological changes are expected to happen outside this envelope.

In order to classify PVCs and other abnormal beats, we can take advantage of the CW parameter estimations provided by the EKF. Since we have the estimations of the CWs, as well as the phase signal, it is possible to have three different polargrams corresponding to P, QRS, and T. In other words, the 2-D vectors  $[\varphi_k P_k]'$ ,  $[\varphi_k C_k]'$ , and  $[\varphi_k T_k]'$  provide three separate polar

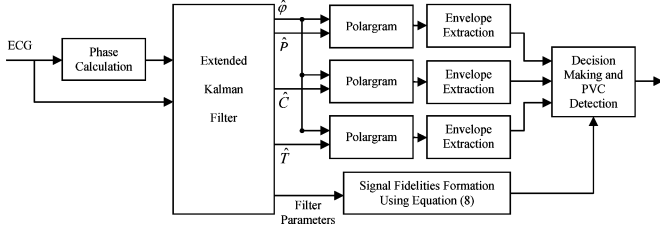


Fig. 2. General block diagram of the proposed PVC detection algorithm.

paths for all time instances,  $k$ . Any morphological changes are detected by monitoring  $\gamma^{CW}$ , and their corresponding envelope  $CW(\theta) \pm 3\sigma_{CW}(\theta)$ . However, to verify the PVCs, one should search the CW polargrams for the absence of a P wave together with the increase in the width of QRS complex and T-wave polar paths. The overall PVC detection algorithm is illustrated in Fig. 2, in which the phase calculation block is simply an R-peak location detector, followed by linear assigning of a phase value between  $-\pi$  and  $\pi$  to the intermediate samples [26]. The decision-making block uses the polargrams and the signal fidelities to detect PVC occurrence. In fact, we use (10) to compute the values of  $\text{thr}^{CW}$  using the  $\gamma^{CW}$  signals. Afterward, the thresholding is performed to locate  $\gamma^{CW}$  peaks. Finally, the polargram is examined for the occurrence of cycles outside the polar envelope in different partitions. If this occurrence holds for all polargrams and the corresponding  $\gamma^{CW}$  passes the threshold, then the beat is determined to be a PVC.

## V. RESULTS

The proposed algorithm was implemented in MATLAB. The MIT-BIH Arrhythmia Database [38], [39] was used for performance evaluation. The performance of the KF is influenced by the initial value for the state vector, as well as the covariance matrices of the process and the measurement noise. Hence, we employ the initialization procedure described in [26] and [31]. Accordingly, the angular frequency  $\omega$ , is set to  $\omega = 2\pi/\overline{T}_{RR}$ , where  $\overline{T}_{RR}$  is the average RR-interval of the whole signal. In order to estimate the initial values for the Gaussian kernels, a typical nonlinear optimization scheme such as the Levenberg–Marquardt procedure [40], [41] is performed on the mean ECG  $[\overline{ECG}(\theta)]$  and the standard deviation  $[\sigma_{ECG}(\theta)]$  [29]. Similarly, the covariance values of  $Q_k$  are found by calculating the magnitude of the deviation of the parameters of the Gaussian functions around the estimated mean that best model the acceptable deviations of the mean ECG within the upper and lower ranges of  $\overline{ECG}(\theta) \pm \sigma_{ECG}(\theta)$ . In a similar manner to [26], we set  $E\{u_k^2\} = (\omega\delta)^2/12$ , and  $E\{u_{2k}^2\}$  to the mean variance of baseline perturbations. The values of  $E\{\eta_{P_k}^2\}$ ,  $E\{\eta_{C_k}^2\}$ , and  $E\{\eta_{T_k}^2\}$  are found from the deviations of the inactive segments of the ECG, around the corresponding CW portion.

Fig. 3 shows a typical ECG signal with PVCs included, the  $\gamma^{CW}$ 's and the polargrams. The envelopes of normal rhythms are also provided, which excludes the PVCs. Visual inspection reveals that these exclusions correspond to the peaks of  $\gamma^{CW}$ , as was expected. Moreover, two PVCs are obvious in all CW polargrams, as well as in all  $\gamma^{CW}$ 's [see Fig. 3(f)–(h)].

As discussed in Section IV,  $\gamma^{CW}$  is sensitive to any morphological changes. However, the benefit of the wave-based model is that it provides three different  $\gamma^{CW}$ 's, each of which monitors the fidelity of the corresponding CW estimation, and is dependant on the corresponding CW rhythm change. Hence, unlike a PVC which imposes a dominant peak in all the  $\gamma^{CW}$ 's, other morphological changes are expected to be tracked in a specific  $\gamma^{CW}$ . Fig. 4 shows the  $\gamma^{CW}$ 's, ECG polargram and the T-polargram for a 17 beats segment of an ECG signal. The segment has two PVCs (third and 11th beats), three aberrated atrial premature beat (fifth, seventh, and 14th beats) and two nonconducted P-wave abnormalities, i.e., blocked atrial premature beats (the last two beats). It can be seen that all the  $\gamma^{CW}$ 's locate the PVC beat, as well as the aberrated atrial premature beat, which have different morphologies compared to the normal cycles. However, these two abnormalities are classified correctly in the polargram, since only the PVC spans outside the envelope. In contrast, the blocked atrial premature beats are identified only in  $\gamma^T$ , and have no effect on the outside of the polargram.

For performance evaluation, we chose 40 ECG records with the same lead configuration, i.e., modified lead II, which contains five types of signals; records with only normal beats (type A), records that contain only normal beats and PVCs (type B), records with no PVCs (type C), records with no normal beats (D), and records consisting normal beats and multiple arrhythmias (type E). We quantified our classifier performance using the most common metrics found in literature: accuracy, sensitivity, and positive predictivity. Accuracy (Ac) is perhaps the most crucial metric for determining overall system performance, and is defined as follows:

$$\text{Ac} = \frac{N_t - N_e}{N_t} \times 100 \quad (11)$$

where  $N_e$  and  $N_t$  represent the total number of classification errors and beats in the file, respectively. To express how successfully a classifier recognizes beats of a certain class without missing them, sensitivity (Sn) is used. Likewise, to measure how exclusively it classifies beats of a certain type, positive predictivity (+P) is used. These two metrics are given by

$$\frac{\text{Sn}}{+P} = \frac{\text{TP}}{\text{TP} + \frac{\text{FN}}{\text{FP}}} \times 100 \quad (12)$$

In these equations, TP, FP, and FN denote true positives, false positives, and false negatives, respectively. Similar to [19], to evaluate the overall performance, the averages are weighted according to the number of beats of each class that were present in a file. The weighted measure is written as

$$M^{WA} = \left( \sum_{i=1}^{n_f} n_{b_i} M_i^{CL} \right) \left( \sum_{i=1}^{n_f} n_{b_i} \right)^{-1}, \quad M \in \{\text{Ac}, \text{Sn}, +P\} \quad (13)$$

where  $n_{b_i}$  is the number of beats for the  $i$ th record,  $n_f$  is the total number of records, and  $M_i^{CL}$  is the value of a specific measure for the  $i$ th record in the class “CL.” The file-by-file

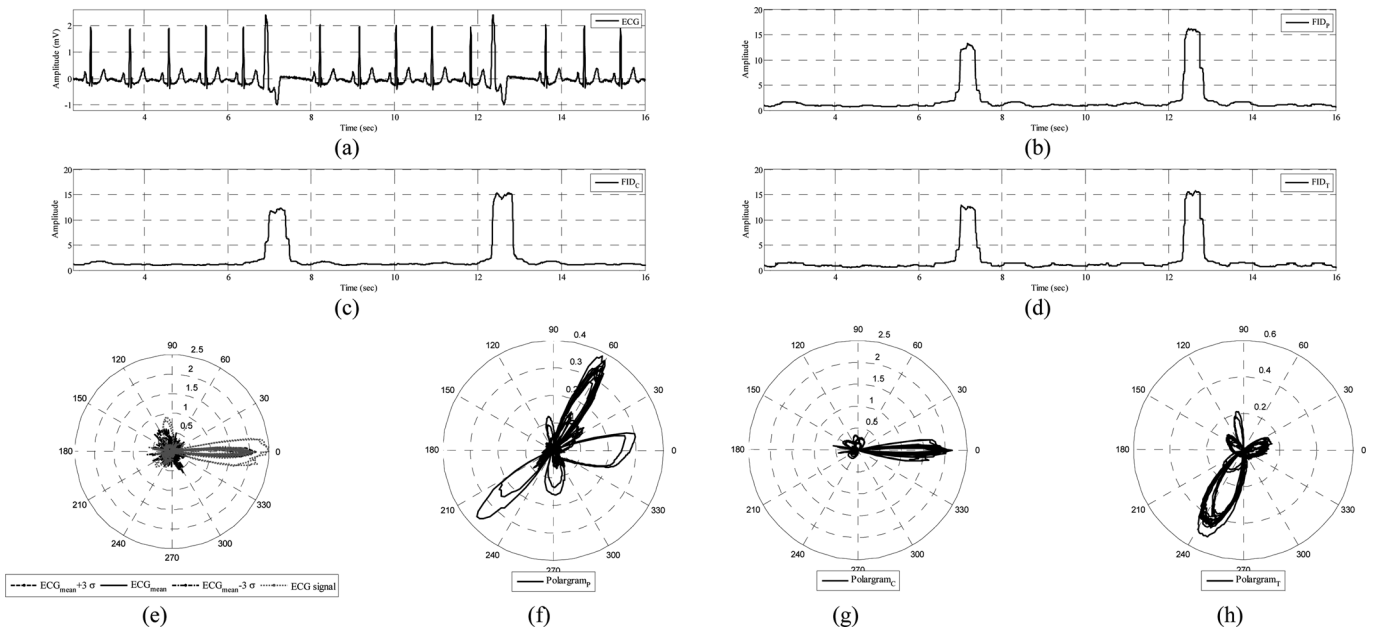


Fig. 3. Elements of PVC monitoring provided by the Bayesian framework. (a) ECG record 119. (b)  $\gamma^P$ . (c)  $\gamma^C$ . (d)  $\gamma^T$ . (e) Signal polargram and the polar envelope. (f) P-wave polargram. (g) QRS complex polargram. (h) T-wave polargram.

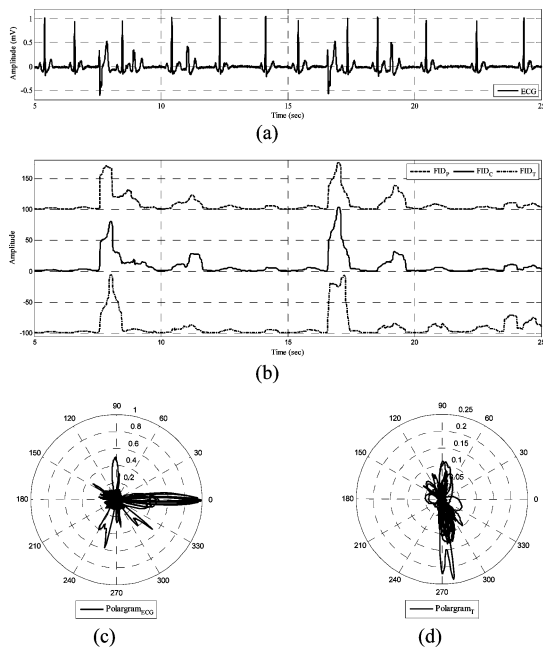


Fig. 4. Effects of PVC, aberrated atrial premature beat and blocked atrial premature beat on signal fidelities and polargram. (a) ECG record 201. (b)  $\gamma^{CW}$  signals. (c) Signal polargram. (d) T-wave polargram.

comprehensive results are provided in Table I. The results show the capability of the proposed wave-based Bayesian framework for PVC identification among other beat types. Performance evaluation results of type A signals show that normal beats are accurately detected. It can be seen that for type B records, where no other abnormality than PVC is presented, the detection algorithm achieves an accuracy, sensitivity, and positive predictivity of 100%. In other words, the algorithm is fully capable of dis-

criminating PVCs and normal beats. Likewise, the results for type C records show that the method is capable of classifying normal beats and other abnormalities in the absence of PVC. In a similar manner, the analysis of type D records illustrates that the algorithm is still reliable for PVC detection, in absence of normal beats. Finally, for type E signals, where a mixture of abnormalities is often presented in the ECG, the PVC detection results are very promising. It can be seen that, in most cases, the sensitivity of PVC detection, as well as the positive predictivity of other beat types, is equal to 100%, which demonstrates that the PVCs are identified with minimum error and the algorithm misses no PVCs. The overall performance evaluation results show a weighted average Sn and +P of 98.77% and 97.47%, respectively. Evaluation results for the identification of other beat types is also well in the acceptable range; however, the polar-envelope-based decision making should be modified to incorporate a wide range of abnormalities, which is beyond the scope of this study.

Furthermore, one should note the impressive results for records 105, 118, 213, 214, 215, and 223, compared to the results reported in [19]. These six records are the most difficult for PVC detection (sensitivity for records 105 and 215 is less than 5%, while others result in Sn  $\approx$  40% [19]). Hence, they are usually excluded from the database [21], [25]. To show the PVC detection capability of our proposed method, we have compared its performance to the file-by-file results of the NN-based approach in [19]. Statistical improvement results are shown in Fig. 5(a). It can be seen that for all cases, the proposed method enhances the mean improvement, while shifting the upper improvement quartile to the positive values. In addition, there are cases whose related improvements are very impressive, and can be followed by the upper side of the error bars, indicating the maximum achieved improvement. Using the numerical evaluation results reported in the reference

TABLE I  
COMPREHENSIVE RESULTS FOR PVC DETECTION USING PROPOSED ALGORITHM

Type	Record	N <sub>t</sub>	Ac (%)	Normal			PVC			Other		
				N <sub>b</sub>	Sn (%)	+P (%)	N <sub>b</sub>	Sn (%)	+P (%)	N <sub>b</sub>	Sn (%)	+P (%)
A	115	1952	100.00	1952	100.00	100.00	0	---	---	0	---	---
	122	2474	100.00	2474	100.00	100.00	0	---	---	0	---	---
B	106	2027	100.00	1507	100.00	100.00	520	100.00	100.00	0	---	---
	119	1987	100.00	1543	100.00	100.00	444	100.00	100.00	0	---	---
	123	1517	100.00	1514	100.00	100.00	3	100.00	100.00	0	---	---
	221	2427	100.00	2031	100.00	100.00	396	100.00	100.00	0	---	---
	230	2255	100.00	2254	100.00	100.00	1	100.00	100.00	0	---	---
C	101	1864	100.00	1859	100.00	100.00	0	---	---	5	100.00	100.00
	103	2083	100.00	2081	100.00	100.00	0	---	---	2	100.00	100.00
	112	2537	99.96	2535	100.00	99.96	0	---	---	2	50.00	100.00
	113	1794	100.00	1788	100.00	100.00	0	---	---	6	100.00	100.00
	117	1534	99.93	1533	100.00	99.93	0	---	---	1	0.00	100.00
	212	2747	99.82	922	99.46	100.00	0	---	---	1825	100.00	99.73
	220	2046	98.10	1952	99.39	98.63	0	---	---	94	87.23	75.23
D	107	2136	99.91	0	---	---	59	96.61	100.00	2077	100.00	99.90
	109	2530	99.96	0	---	---	38	100.00	97.44	2492	99.96	100.00
	118	2277	100.00	0	---	---	16	100.00	100.00	2261	100.00	100.00
	214	2260	100.00	0	---	---	256	100.00	100.00	2004	100.00	100.00
E	100	2271	99.43	2237	100.00	99.42	1	100.00	100.00	33	60.61	100.00
	102	2185	98.81	99	100.00	79.20	4	100.00	100.00	2082	98.75	100.00
	105	2572	99.30	2501	100.00	100.00	41	100.00	69.50	30	40.00	100.00
	114	1879	99.79	1820	100.00	99.89	43	100.00	100.00	16	75.00	100.00
	116	2411	99.50	2301	99.87	100.00	109	91.74	97.09	1	100.00	100.00
	121	1862	99.95	1860	100.00	99.95	1	100.00	100.00	1	0.00	100.00
	200	2600	98.88	1742	100.00	98.36	826	100.00	100.00	32	9.37	100.00
	201	1963	98.11	1625	100.00	98.60	198	95.96	93.60	140	79.28	93.27
	202	2135	98.59	2060	100.00	98.89	19	89.47	77.27	56	50.00	93.33
	203	2979	98.19	2528	98.10	99.68	444	97.35	91.49	7	57.14	22.22
	205	2655	99.81	2570	100.00	99.80	71	100.00	100.00	14	64.28	100.00
	208	2953	92.92	1585	98.93	89.14	992	99.90	100.00	376	49.20	91.13
	210	2648	98.86	2421	99.83	99.26	194	98.97	96.97	33	27.27	60.00
	213	3249	96.74	2639	100.00	100.00	220	95.90	68.50	390	75.13	97.02
	215	3361	98.93	3194	99.47	100.00	164	88.41	100.00	3	100.00	8.33
	217	2208	96.47	244	83.20	100.00	162	98.76	82.05	1802	98.06	97.62
	219	2154	99.40	2082	100.00	99.38	64	89.06	100.00	8	25.00	100.00
	223	2604	95.77	2028	96.74	98.34	473	97.67	100.00	103	67.96	51.47
	228	2053	98.88	1688	98.87	99.88	362	99.45	100.00	3	33.33	4.55
	231	1570	98.92	314	100.00	94.59	2	100.00	100.00	1254	98.64	100.00
233	3077	99.90	2229	100.00	100.00	830	100.00	100.00	18	83.33	100.00	
234	2752	99.38	2699	100.00	99.37	3	100.00	100.00	50	66.00	100.00	
<b>Total</b>		92588	---	68411	---	---	6956	---	---	17221	---	---
<b>Mean</b>		2314.7	<b>99.10</b>	1710.27	89.35	88.81	1739.0	75.98	74.35	4305.2	57.39	72.34
<b>Standard Deviation</b>		---	1.44	---	30.28	30.20	---	41.58	41.32	---	39.58	41.67
<b>Weighted Average</b>		---	<b>99.01</b>	---	<b>99.66</b>	<b>99.38</b>	---	<b>98.77</b>	<b>97.47</b>	---	<b>96.54</b>	<b>98.81</b>

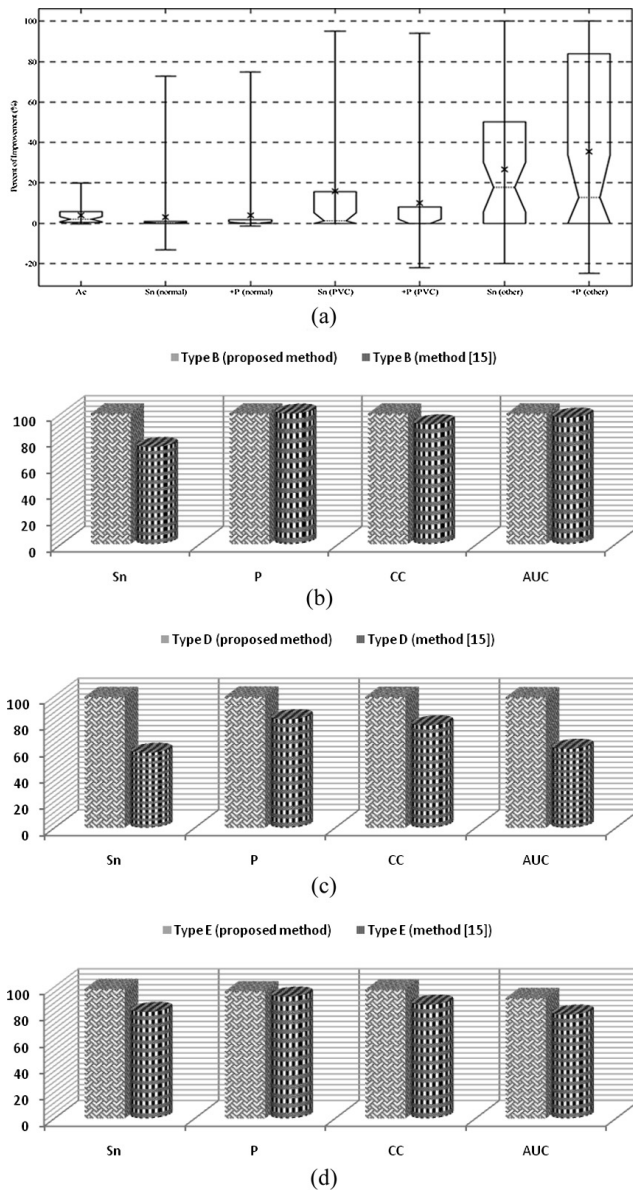


Fig. 5. Performance comparison of the proposed method to the wavelet-based NN algorithm [17], evaluated on the same 40 records from MIT-BIH Arrhythmia Database. (a) Improvement statistics for the whole database shown with box plots. The box lines show the lower quartile, median (dotted lines) and upper quartile improvement values, and the error bars indicate the min and max improvement values. The mean improvement is shown with a cross symbol. (b)–(d) Comparative results for PVC detection using type B, type D, and type E signals, respectively. The results of our proposed method are shown by box bars while those of [19] are shown with cylindrical bars.

paper [19], it is also possible to compute the correlation coefficient (CC) as

$$CC = \frac{1}{2} \left( 1 + \frac{(TP)(TN) - (FP)(FN)}{\sqrt{(TP + FN)(TN + FP)(TP + FP)(TN + FN)}} \right) \quad (14)$$

where TN represents the number of elements predicted as false that are false (true negatives). The ratio in (14) scores positively correct predictions and negatively incorrect ones, and takes a value between  $-1$  and  $1$ . Accordingly, the CC measure falls

into the interval of  $[0, 1]$ . The more correct the method is, the closer CC would be to unity. Another metric for measuring the correctly predicted elements is specificity (Sp), given by

$$Sp = \frac{TN}{FP + TN} \times 100. \quad (15)$$

Having computed the values of Sn and Sp, a plot of Sn versus Sp, namely the receiver operating characteristic (ROC) curve, is built for the same classification method using a series of detection results. However, since we do not vary the filter parameters and we have no thresholds to obtain stepwise Sn and Sp values, the best classification method is the one that describes the largest area under the curve (AUC).

In order to investigate the true positive PVC detection performance, we have chosen types B, D, and E signals for analysis. Fig. 5(b)–(d) shows the mean values of different metrics for these types of records, evaluated using the proposed method (box bars) and the NN-based technique [19] (cylindrical bars). The figure illustrates that in contrast to the NN-based method, all metrics' values for the proposed algorithm are over 90%, and are often very close to 100%.

Furthermore, the improvement in PVC detection is obvious by visual comparison of the height of cylindrical bars to that of box bars. Specifically, we note the improvement in sensitivity, which demonstrates that the Bayesian method has much fewer FN detections. Hence, the minimum number of PVCs is misclassified by the proposed approach. In other words, unlike the method in [19], which is based on feature extraction and NN classification with no temporal memory, our proposed technique benefits from the tracking potential of the Bayesian framework to obtain much better detection accuracies for PVCs.

To appreciate the merits of the proposed method over conventional PVC classification algorithms and to ensure its ability to locate PVCs, we have compared our results to those of some benchmark techniques in the literature. The results are reported in Table II. Since the results of methods are reported for different databases, we have also provided the number of ECG records ( $N_{rec}$ ) and number of PVCs ( $N_{PVC}$ ) used in each method. It can be seen from Table II that our proposed method provides a higher Ac and Sn, while preserving the  $+P$  in the acceptable range. Additionally, taking the number of analyzed PVCs into consideration, the  $+P$  results of our algorithm is comparable to and usually superior to the other methods, which shows the ability of the proposed framework to distinguish the PVCs from other beat types more accurately.

Another interesting feature of the proposed method is that the PVC detection depends upon both the  $\gamma^{CW}$  and the polar envelope, which together enables the algorithm to distinguish between PVCs and rhythms with similar morphologies, which is a significant problem in feature-based methods. As an example, previous studies could not distinguish between PVCs and left bundle branch blocks (LBBBs) beats [19], [21]. LBBB is a cardiac conduction abnormality seen on ECG, in which activation of the left ventricle is delayed, which results in the left ventricle contracting later than the right ventricle. The criteria to diagnose an LBBB are QRS widening and T-wave discordance, in which the T wave should be deflected opposite the terminal deflection

TABLE II  
PERFORMANCE COMPARISON OF BENCHMARK METHODS FOR PVC DETECTION TO PROPOSED MODEL-BASED METHOD

Detection Strategy	Method	Database		Performance measures		
		N <sub>rec</sub>	N <sub>PVC</sub>	Ac (%)	Sn (%)	+P (%)
Time-domain statistics	Moody <i>et al</i> [5]	20	5677	---	91.90	89.46
		44	6731	---	74.51	97.36
PCA	Moody <i>et al</i> [6]	20	5677	---	93.12	94.76
		44	6731	---	92.73	96.92
Neural networks	Inan <i>et al</i> [19]	40	6958	95.20	85.20	92.40
	Ince <i>et al</i> [20]	40	6958	97.00	93.40	93.30
	Shyu <i>et al</i> [21]	7	953	97.04	96.67	97.04
KNN classifier	Christov <i>et al</i> [23]	20	5677	---	97.30	97.70
Gaussian process	Melgani and Bazi [25]	18	2720	97.10	97.60	97.00
		27	4080	96.90	84.70	97.50
Bayesian filtering	Proposed	40	6956	99.10	98.77	97.47

of the QRS complex. This is similar to PVC; however, in the case of a PVC, the P wave is fused in the QRS complex and the dominant T wave is not essentially deflected opposite the terminal deflection of the QRS complex. Hence, using the time interval features and an NN [17] or wavelet features and fuzzy NN [21], it is very difficult to distinguish between a PVC and an LBBB beat. For instance, Shyu *et al.* [21] reported 405 LBBB as FN detections while characterizing PVCs. The potential of the Bayesian framework enables it to correctly identify LBBB as non-PVCs. This is due to the polar envelope formation based on the LBBB, which spans a different partition from the PVCs. Specifically,  $\gamma^{CW}$  identifies the LBBB as a monotone rhythm in ECG, whereas the PVC is characterized as a rhythm change. This is obvious by comparing the results of our algorithm for record 214 (Sn = 100%, +P = 100%) to the reported results of [19] for the same record (Sn = 47.66%, +P = 92.42%), which includes 256 PVCs and 1996 LBBB beats. Fig. 6 illustrates a segment of record 214, the signal and T-wave polargrams and the signal fidelity  $\gamma^T$  corresponding to the T wave.

## VI. DISCUSSION AND CONCLUSION

In this paper, a wave-based Bayesian framework was presented and validated for PVC beat detection that is capable of running on a single ECG lead. The method is based on an EKF algorithm that incorporates the characteristic waves of the ECG into a dynamical model. By separating the Gaussian functions, and using two kernels for each asymmetric wave, a state-space model was constructed. The proposed set of equations aims at integrating into the ECG model a mechanism that estimates an ECG signal as a combination of finite characteristic waveforms, each of which represents a particular physiological state of the heart. According to this specific model, the EKF structure provides a means of tracking the behavior of the CWs, throughout the filtering procedure.

From a filtering point of view, KFs can be thought of as adaptive filters that continuously move the location of the poles and zeros of their transfer functions, according to the signal or noise content of the input observations and the prior model of the signal dynamics. The filter structure is based upon a

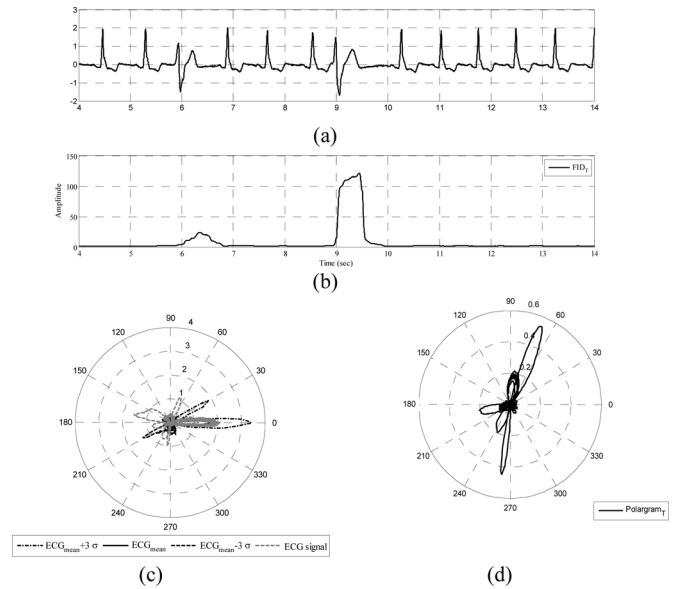


Fig. 6. Distinguishing LBBB and PVCs for a typical ECG signal. (a) ECG record 214. (b)  $\gamma^T$ . (c) Signal polargram and the polar envelope. (d) T-wave polargram.

unique dynamical model, which is adapted to the observations according to the propagation equations. In this way, we can track the reliability of the estimations, as well as the fidelity of the filter. Moreover, this feature allows the filter to adapt with different spectral shapes and temporal nonstationarities, since the variance of the observation noise in (4) represents the degree of reliability of a single observation, as well as the degree of adaptively tracking the input noisy measurement. Based on this concept, we introduced the signal fidelity,  $\gamma^{CW}$ , corresponding to each CW, and monitored these parameters to detect PVC occurrence. Furthermore, a polar representation was introduced to distinguish between the rhythm changes that occur inside the polar envelope and PVCs, which span a different portion of the polargram. The designed filter was applied to standard ECG databases, and compared to other published methods. The results demonstrate the filter's capability in tracking the PVCs. It was also shown that the  $\gamma^{CW}$ 's are capable of discrimination between PVCs and other abnormalities that exhibit a defect in a specific CW. However, for those abnormalities that affect the  $\gamma^{CW}$ 's the same manner as would a PVC, the polargram is used to verify the occurrence outside the polar envelope.

Performance evaluation results showed that the developed method provides a reliable and accurate PVC detection, providing an accuracy of 98.83%, weighted average specificity of 99.29% for normal and 98.43% for PVC, and a mean positive predictivity of 99.75% for normal and 96.68% for PVC, which is well within the acceptable range, and is superior to the previously reported results. Moreover, in comparison to other published methods for PVC detection, our proposed approach provides a superior performance, and there is no need to employ decision rules based on comparison against thresholds, feature extraction, training, and selection of the classifiers' structure. Another point of interest is the capability of the algorithm to

fully determine the PVCs, with Ac, Sn, and +P equal to 100%, for the records that contain only two specific beat types: normal sinus beats and PVCs. It was also shown that the proposed method is applicable to reliable PVC detection in presence of other abnormalities, and in particular, left bundle branch block.

It should be noted that the initial value for the state vector as well as the selection of the covariance matrices of the process and the measurement noise will influence the trajectory of the estimated vectors. The dependence of the results on these initial estimations is the major drawback of the proposed method. Hence, an automated procedure for reliable initialization was proposed. Although the Bayesian method we present depends on the initial values, the method is still more efficient compared to NN-based approaches since the initialization and training of the EKF parameters can be performed using just a few early cycles.

Due to the recursive structure of the KF, the proposed method is also computationally tractable and of special interest for real-time applications. Generally, the computation time of this method is linearly proportional to the signal length in samples. For the currently developed MATLAB code, the computation time is already close to real time using a Core Duo 1.86-GHz CPU. Compilation and optimization of this code, or conversion into a low-level language for use in pre-processing units of clinical monitoring systems would result in a significant increase in performance speed. This would allow the algorithm to run on multiple ECG leads in real time on most embedded systems that are increasingly available with on-board DSP chipsets.

#### REFERENCES

- [1] American Heart Association. *Heart Disease and Stroke Statistics—2009 Update*. Dallas, TX: American Heart Association, 2009.
- [2] I. Atsushi, M. Hwa, A. Hassankhani, T. Liu, and S. M. Narayan, "Abnormal heart rate turbulence predicts the initiation of ventricular arrhythmias," *Pacing Clin. Electrophysiol.*, vol. 11, pp. 1189–1197, 2005.
- [3] R. Schneider, P. Barthel, and M. Watanabe, "Heart rate turbulence on Holter," in *Dynamic Electrocardiography*, M. Malik and A. J. Camm, Eds. New York: Futura, 2004, ch. 20, pp. 190–193.
- [4] D. Dubin, *Rapid Interpretation of EKG's*, 5th ed. Tampa, FL: Cover, 2000.
- [5] G. B. Moody and R. G. Mark, "Development and evaluation of a 2-lead ECG analysis program," in *Proc. Comput. Cardiol.*, 1982, pp. 39–44.
- [6] P. D. Chazal, M. O'Dwyer, and R. B. Reilly, "Classification of heartbeats using ECG morphology and heartbeat interval features," *IEEE Trans. Biomed. Eng.*, vol. 51, no. 7, pp. 1196–1206, Jul. 2004.
- [7] G. B. Moody and R. G. Mark, "QRS morphology representation and noise estimation using the Karhunen–Loève transform," in *Proc. Comput. Cardiol.*, 1989, pp. 269–272.
- [8] W. T. Cheng and K. L. Chan, "Classification of electrocardiogram using hidden markov models," in *Proc. 20th Annu. Int. Conf. IEEE EMBS*, 1998, vol. 20, pp. 143–146.
- [9] D. A. Coast, R. M. Stern, G. G. Cano, and S. A. Briller, "An approach to Cardiac arrhythmia analysis using hidden Markov models," *IEEE Trans. Biomed. Eng.*, vol. 37, no. 9, pp. 826–835, Sep. 1990.
- [10] R. V. Andreão, B. Dorizzi, and J. Boudy, "ECG signal analysis through hidden Markov models," *IEEE Trans. Biomed. Eng.*, vol. 53, no. 8, pp. 1541–1549, Aug. 2006.
- [11] M. R. Risk, J. F. Sobh, and J. P. Saul, "Beat detection and classification of ECG using self organizing maps," in *Proc. 19th Int. Conf. IEEE EMBS*, 1997, vol. 19, pp. 89–91.
- [12] L. Senhadji, G. Carrault, J. J. Bellanger, and G. Passariello, "Comparing wavelet transforms for recognizing cardiac patterns," *IEEE Eng. Med. Biol. Mag.*, vol. 14, no. 2, pp. 167–173, Mar./Apr. 1995.
- [13] X. Alfonso and T. Q. Nguyen, "ECG beat detection using filter banks," *IEEE Trans. Biomed. Eng.*, vol. 46, no. 2, pp. 192–202, Feb. 1999.
- [14] P. D. Chazal, M. O'Dwyer, and R. B. Reilly, "Automatic classification of heartbeats using ECG morphology and heartbeat interval features," *IEEE Trans. Biomed. Eng.*, vol. 51, no. 7, pp. 1196–1206, Jul. 2004.
- [15] H. G. Hosseini, D. Luo, and K. J. Reynolds, "The comparison of different feed forward neural network architectures for ECG signal diagnosis," *Med. Eng. Phys.*, vol. 28, pp. 372–378, 2006.
- [16] F. M. Ham and S. Han, "Classification of cardiac arrhythmias using fuzzy ARTMAP," *IEEE Trans. Biomed. Eng.*, vol. 43, no. 4, pp. 425–430, Apr. 1996.
- [17] I. Christov and G. Bortolan, "Ranking of pattern recognition parameters for premature ventricular contractions classification by neural networks," *Physiol. Meas.*, vol. 25, pp. 1281–1290, 2004.
- [18] G. Bortolan, I. Jekova, and I. Christov, "Comparison of four methods for premature ventricular contraction and normal beat clustering," in *Proc. Comp. Cardiol.*, 2005, vol. 32, pp. 921–924.
- [19] O. T. Inan, L. Giovangrandi, and G. T. A. Kovacs, "Robust neural-network-based classification of premature ventricular contractions using wavelet transform and timing interval features," *IEEE Trans. Biomed. Eng.*, vol. 53, no. 12, pp. 2507–2515, Dec. 2006.
- [20] T. Ince, S. Kiranyaz, and M. Gabbouj, "Automated patient-specific classification of premature ventricular contractions," in *Proc. 30th Int. Conf. IEEE EMBS*, 2008, pp. 5474–5477.
- [21] L. Y. Shyu, Y. H. Wu, and W. Hu, "Using wavelet transform and fuzzy neural network for VPC detection from the Holter ECG," *IEEE Trans. Biomed. Eng.*, vol. 51, no. 7, pp. 1269–1273, Jul. 2004.
- [22] J. Zhou, "Automatic detection of premature ventricular contraction using quantum neural networks," in *Proc. BIBE*, 2003, pp. 1–5.
- [23] I. Christov, I. Jekova, and G. Bortolan, "Premature ventricular contraction classification by the Kth nearest-neighbours rule," *Physiol. Meas.*, vol. 26, pp. 123–130, 2005.
- [24] L. Zhao, M. Wiggins, and G. Vachtsevanos, "Premature ventricular contraction beat detection based on symbolic dynamics analysis," in *Proc. IASTED*, 2003, pp. 48–50.
- [25] F. Melgani and Y. Bazi, "Detecting premature ventricular contractions in ECG Signals with Gaussian processes," in *Proc. Comp. Cardiol.*, 2008, vol. 35, pp. 237–240.
- [26] R. Sameni, M. B. Shamsollahi, C. Jutten, and G. D. Clifford, "A nonlinear Bayesian filtering framework for ECG denoising," *IEEE Trans. Biomed. Eng.*, vol. 54, no. 12, pp. 2172–2185, Dec. 2007.
- [27] R. Sameni, M. B. Shamsollahi, and C. Jutten, "Model-based Bayesian filtering of cardiac contaminants from biomedical recordings," *Physiol. Meas.*, vol. 29, pp. 595–613, 2008.
- [28] P. E. McSharry, G. D. Clifford, L. Tarassenko, and L. A. Smith, "A dynamic model for generating synthetic electrocardiogram signals," *IEEE Trans. Biomed. Eng.*, vol. 50, no. 3, pp. 289–294, Mar. 2003.
- [29] G. D. Clifford, A. Shoeb, P. E. McSharry, and B. A. Janz, "Model-based filtering, compression and classification of the ECG," *Int. J. Bioelectromagn.*, vol. 7, no. 1, pp. 158–161, 2005.
- [30] O. Sayadi, R. Sameni, and M. B. Shamsollahi, "ECG denoising using parameters of ECG dynamical model as the states of an extended Kalman filter," in *Proc. 29th Int. Conf. IEEE EMBS*, 2007, pp. 2548–2551.
- [31] O. Sayadi and M. B. Shamsollahi, "ECG denoising and compression using a modified extended Kalman filter structure," *IEEE Trans. Biomed. Eng.*, vol. 55, no. 9, pp. 2240–2248, Sep. 2008.
- [32] O. Sayadi and M. B. Shamsollahi, "A model-based Bayesian framework for ECG beat segmentation," *Physiol. Meas.*, vol. 30, pp. 335–352, 2009.
- [33] A. Gelb, *Applied Optimal Estimation*. Cambridge, MA: MIT Press, 1974.
- [34] S. M. Kay, Ed., *Fundamentals of Statistical Signal Processing: Estimation Theory*. Englewood Cliffs, NJ: Prentice Hall PTR, 1993.
- [35] D. Simon, Ed., *Optimal State Estimation*. New York: Wiley, 2006.
- [36] S. Haykin, Ed., *Kalman Filtering and Neural Networks*. New York: Wiley, 2001.
- [37] M. S. Grewal, L. R. Weill, and A. P. Andrews, Eds., *Global Positioning Systems, Inertial Navigation, and Integration*. New York: Wiley, 2001.
- [38] *The MIT-BIH Arrhythmia Database*. (2009, Jun. 13). [Online]. Available: <http://physionet.org/physiobank/database/mitdb/>
- [39] A. L. Goldberger, L. A. N. Amaral, L. Glass, J. M. Hausdorff, P. Ch. Ivanov, R. G. Mark, J. E. Mietus, G. B. Moody, C.-K. Peng, and H. E. Stanley. (2000, Jun. 13). "PhysioBank, PhysioToolkit, and PhysioNet: components of a new research resource for complex physiologic signals," *Circulation*. [Online]. 101(23), pp. e215–e220. Available: <http://circ.ahajournals.org/cgi/content/full/101/23/e215>
- [40] K. Levenberg, "A method for the solution of certain problems in least squares," *Quart. Appl. Math.*, vol. 2, pp. 164–168, 1944.
- [41] D. Marquardt, "An algorithm for least squares estimation of nonlinear parameters," *SIAM J. Appl. Math.*, vol. 11, pp. 431–441, 1963.